

Article

Bi-Polymer Electrospun Nanofibers Embedding Ag₃PO₄/P25 Composite for Efficient Photocatalytic Degradation and Anti-Microbial Activity

Zunaira Habib ¹, Chang-Gu Lee ², Qilin Li ^{3,4}, Sher Jamal Khan ^{1,*}, Nasir Mahmood Ahmad ⁵, Yousuf Jamal ¹, Xiaochuan Huang ³ and Hassan Javed ⁶

¹ Institute of Environmental Sciences and Engineering, National University of Sciences and Technology (NUST), Islamabad 44000, Pakistan; zhabib.phdiese@student.nust.edu.pk (Z.H.); yousuf.jamal@iese.nust.edu.pk (Y.J.)

² Department of Environmental and Safety Engineering, Ajou University, Suwon 16499, Korea; changgu@ajou.ac.kr

³ Department of Civil and Environmental Engineering, Rice University, 6100 Main Street MS 519, Houston, TX 77005, USA; qilin.li@rice.edu (Q.L.); xiaochuan.huang@rice.edu (X.H.)

⁴ NSF Nanosystem Engineering Research Center for Nanotechnology Enabled Water Treatment, 6100 Main Street MS 6398, Houston, TX 77005, USA

⁵ Polymer Research lab, School of Chemical and Materials Engineering, National University of Sciences and Technology (NUST), Islamabad 44000, Pakistan; nasir.ahmad@scme.nust.edu.pk

⁶ Department of Chemistry, Rice University, 6100 Main Street MS 6398, Houston, TX 77005, USA; hassan.javed@rice.edu

* Correspondence: s.jamal@iese.nust.edu.pk or sherjamal77@gmail.com; Tel.: +92-51-90854353

Received: 20 April 2020; Accepted: 15 May 2020; Published: 14 July 2020



Abstract: Using a bi-polymer system comprising of transparent poly(methyl methacrylate) (PMMA) and poly(vinyl pyrrolidone) (PVP), a visible light active Ag₃PO₄/P25 composite was immobilized into the mats of polymeric electrospun nanofibers. After nanofibers synthesis, sacrificial PVP was removed, leaving behind rough surface nanofibers with easy access to Ag₃PO₄/P25 composite. The remarkable photocatalytic efficiency was attained using a PMMA and Ag₃PO₄/P25 weight ratio of 1:0.6. Methyl orange (MO) was used to visualize pollutant removal and exhibited stable removal kinetics up to five consecutive cycles under simulated daylight. Also, these polymeric nanofibers (NFs) revealed an important role in the destruction of microorganisms (*E. coli*), signifying their potential in water purification. A thin film fibrous mat was also used in a small bench scale plug flow reactor (PFR) for polishing of synthetic secondary effluent and the effects of inorganic salts were studied upon photocatalytic degradation in terms of total organic carbon (TOC) and turbidity removal. Lower flow rate (5 mL/h) resulted in maximum TOC and turbidity removal rates of 86% and 50%, respectively. Accordingly, effective Ag₃PO₄/P25 immobilization into an ideal support material and selectivity towards target pollutants could both enhance the efficiency of photocatalytic process under solar radiations without massive energy input.

Keywords: Ag₃PO₄/P25; *Escherichia coli*; methyl orange; nanofibers; photocatalytic degradation; plug flow reactor; inorganic salts

1. Introduction

Among various water treatment techniques, photocatalysis has been extensively studied for its potential in water purification using solar radiations without chemical addition. Among the large

number of photocatalysts that have been explored, TiO_2 based nanomaterials are most attractive due to their low cost, mechanical robustness, non-toxic nature, chemical stability, and capability to completely mineralize organic pollutants [1]. However, several challenges exist in the application of TiO_2 nanomaterials in water and wastewater treatment, including (1) low quantum efficiency due to electron-hole pair recombination, (2) the need for down-stream separation to recover TiO_2 nanomaterials from water if a TiO_2 suspension is used, (3) aggregate formation in aqueous phase, and (4) the need for UV light activation due to their large band gap [2]. The large band gap (~3.2 eV for anatase) of TiO_2 determines that it can only be activated by UV light, demanding significant energy input [3]. An attractive strategy to lower the energy consumption of TiO_2 -based photocatalysis is to develop photocatalysts which retaliate visible light, a large portion of energy in solar irradiation [4].

Three strategies have been explored to broaden the absorption spectrum to visible range, including (i) doping TiO_2 with metals and non-metals elements, (ii) TiO_2 composites with organic and inorganic compounds and (iii) developing new semiconductor photocatalysts with the ability to absorb visible light [5]. Among narrow band gap metal oxides coupled with TiO_2 , Yi and his coworkers reported a breakthrough in using $\text{Ag}_3\text{PO}_4/\text{TiO}_2$ as a visible light-active photocatalyst. They reported that photocatalytic activity of $\text{Ag}_3\text{PO}_4/\text{TiO}_2$ is superior than pure Ag_3PO_4 and TiO_2 nanoparticles, which may be attributed to the unique band positions of these two semiconductors [6].

To resolve the problem associated with the additional cost for separating nanophotocatalyst from water [7], immobilization of photocatalyst onto an adequate substrate can be considered alternatively. The ideal support material for immobilization of photocatalyst must provide firm anchoring to avoid nanoparticle leaching, mechanical stability and selective affinity towards target pollutants. Numerous materials have been studied as photocatalyst supports, including activated carbon, glass, stainless steel, alumina, silica, zeolite, ceramic and polymers [8]. From these materials, polymeric materials offer strong immobilizing capability as well as chemical and mechanical stability. In this context, electrospun nanofibers have gained much attention as a low-cost and effective way to immobilize nanophotocatalysts. Among the currently available strategies for fabrication of one-dimensional electrospun nanofibers, electrospinning is one of the most versatile and highly adopted approach due to its cost-effective setup [9]. Kalantari et al. [10] illustrated that it requires a syringe pump, a source of high electric current and a stainless-steel collector (connected to the ground) to collect the nanofibers. The schematic illustration of electrospinning apparatus is shown in Figure 1. However, nanoparticle immobilization in polymers is challenging due to loss of active sites, which results in lower photocatalytic efficiency [11].

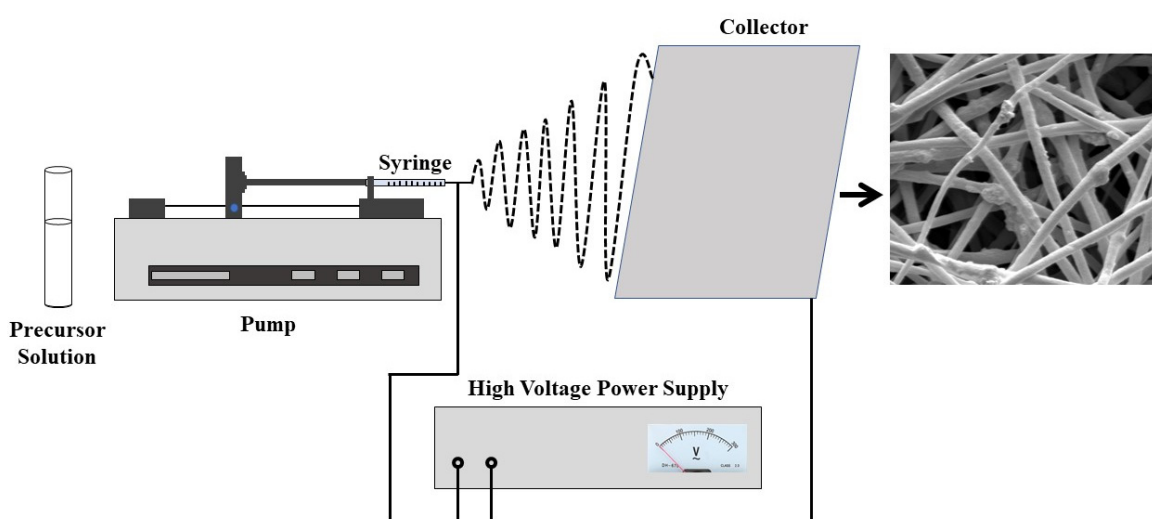


Figure 1. Schematic illustration of electrospinning process.

In this work, a novel study is reported on the facile synthesis of poly(methyl methacrylate) (PMMA) nanofibers (NFs) containing $\text{Ag}_3\text{PO}_4/\text{P}25$ nanoparticles. These polymer fibers act as a strong substrate with exposed $\text{Ag}_3\text{PO}_4/\text{P}25$ nanoparticles to considerably enhance pollutants contact to anchored nanoparticles. This strategy was achieved using the polymer blending approach where immediately after electrospinning, one of the polymers was removed via selective dissolution. For this purpose, poly(vinyl pyrrolidone) (PVP), a water soluble polymer was used with PMMA. Using biopolymer system, idea of PVP dissolution in pure water (in order to expose nanoparticles on the surface of NFs) can be considered novel and is not reported earlier. Also, the NFs prepared of this specific polymer blend have not been used earlier to anchor the $\text{Ag}_3\text{PO}_4/\text{P}25$ nanocomposite. After dipping in water, PVP was easily washed away, leaving behind a lumpy surface exposed with nanoparticles. The choice of using PMMA as a hosting matrix was attributed to its mechanical properties, transparent to visible light, economical, environmentally stable and facile electropinnability that is helpful in obtaining homogeneous nanofibers [12]. PMMA is also important in improving and introducing novel properties to the fibers for their multiple uses in the field of water remediation. The foremost objective of this study was to synthesize composite NFs with $\text{Ag}_3\text{PO}_4/\text{P}25$ nanoparticles exposed on the surface as well as easily separable and recyclable. First, these NFs were evaluated for photodegradation of individual dye simulated textile effluent along with its capability to kill microorganisms (bacteria). Then, a thin film NF mat with efficient photocatalytic capacity was used in a plug flow reactor (PFR) for the polishing (as a tertiary treatment option) of synthetic up-flow anaerobic sludge blanket (UASB) effluent, [13] previously studied at the Institute of Environmental Sciences and Engineering, NUST, Islamabad, Pakistan.

2. Results and Discussion

2.1. Characterization of Synthesized Nanofibers

Electrospinning offers a versatile approach for the large-scale production of NFs [14]. Before evaluating the photocatalytic and antibacterial activity of prepared NFs, samples were characterized morphologically and structurally. Figure 2 shows SEM images of pure polymer blend (PMMA/PVP) NFs and polymer NFs having $\text{Ag}_3\text{PO}_4/\text{P}25$ nanoparticles immobilized on the surface with a blending ratio of PMMA (12%) and PVP (6%). The fibers are mostly bead free (Figure 2a) with the typical random orientation commonly seen in electrospun NFs. Conversely, before removing sacrificial PVP, smooth surface NFs were observed with hardly visible nanoparticles (Figure 2b). However, after PVP removal via washing, the overall morphology of NFs was not destroyed except for bead formation (small bumps), which represents nanoparticle aggregation (Figure 2c). Pure polymer NFs had an average diameter of 285 ± 93 nm. However, after adding nanoparticles into the polymer blend (before PVP removal), an increase in diameter (485 ± 240 nm) was observed due to encapsulated nanoparticles in the polymer matrix. Subsequently, the removal of sacrificial PVP resulted in NFs having a rougher surface morphology with an average diameter of 587 ± 182 nm. The increase in diameter was an upshot of exposed nanoparticles upon the outer surface of NFs, as stated in the literature [15]. A similar trend was found in a previous study where increase in diameter was observed upon adding TiO_2 to the polymer [16]. This fact was further confirmed by EDX analysis with more pronounced signals of deposited nanoparticles after washing.

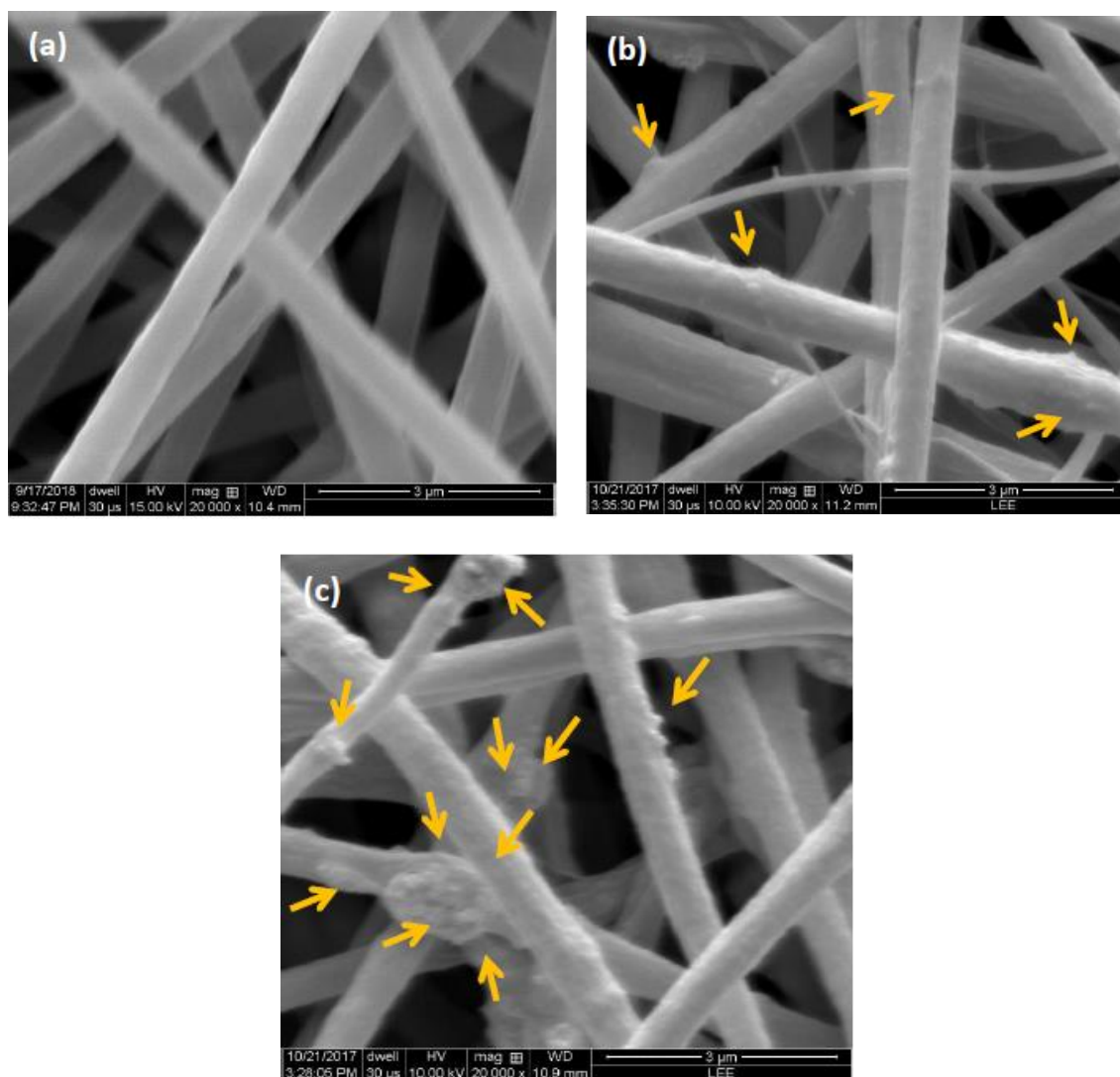


Figure 2. SEM images of electrospun nanofibers **(a)** poly(methyl methacrylate)/poly(vinyl pyrrolidone) (PMMA/PVP), **(b)** PMMA/PVP- Ag_3PO_4 /P25 before washing, and **(c)** PMMA/PVP- Ag_3PO_4 /P25 after washing.

Furthermore, the EDX study of NFs (Figure 3) illustrated significantly sharp peaks after PVP removal, which corresponds to the fact that nanoparticles have more access to the surface of NFs. Furthermore, the EDX study revealed the purity of NFs, as no traces of other elemental impurities were detected in the sample.

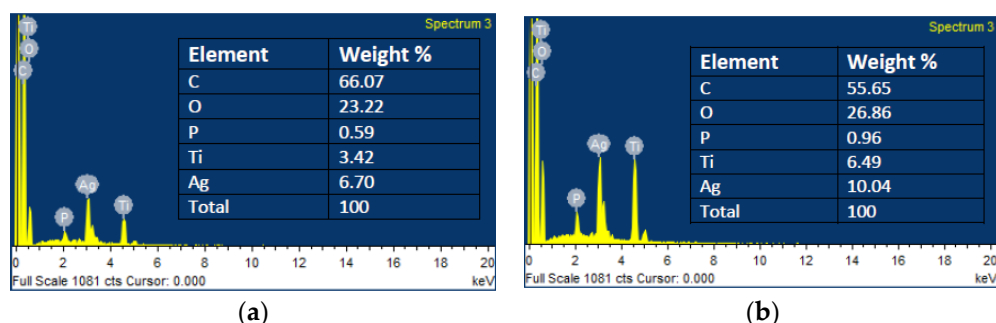


Figure 3. EDX spectra of PMMA/PVP- Ag_3PO_4 /P25 nanofibers before **(a)** and after washing **(b)**.

Figure 4 shows the FTIR spectra of $\text{Ag}_3\text{PO}_4/\text{P}25$ NFs before and after washing with water for PVP removal. It is noted that both spectra showed characteristic peaks of PMMA at 1730 ($\text{C}=\text{O}$), 1150 ($-\text{O}-\text{CH}_3$), and 868 ($\text{C}-\text{O}-\text{C}$) cm^{-1} [17]. The difference in spectra was the characteristic peaks of PVP with dotted lines. PVP exhibited sharp peak at 1660 cm^{-1} due to carbonyl ($-\text{C}=\text{O}$) stretching that was not shown in NFs after dipping in water for its removal [18]. The peaks at 1270 and 3400 cm^{-1} were attributed to stretching vibration in the amide ($-\text{CN}$) group and hydroxyl ($\text{O}-\text{H}$) group, respectively [19]. As synthesized NFs have $\text{Ag}_3\text{PO}_4/\text{P}25$ composite, absorption peaks at 1400 and 1050 cm^{-1} were attributed to the stretching vibration of double bonded oxygen ($\text{P}=\text{O}$), as well as the molecular vibration of PO_4^{3-} ($\text{P}-\text{O}$) [20]. Besides this, another peak slightly higher in the washed sample at 947 cm^{-1} exhibited strong interaction among Ag_3PO_4 and P25 nanoparticles [21].

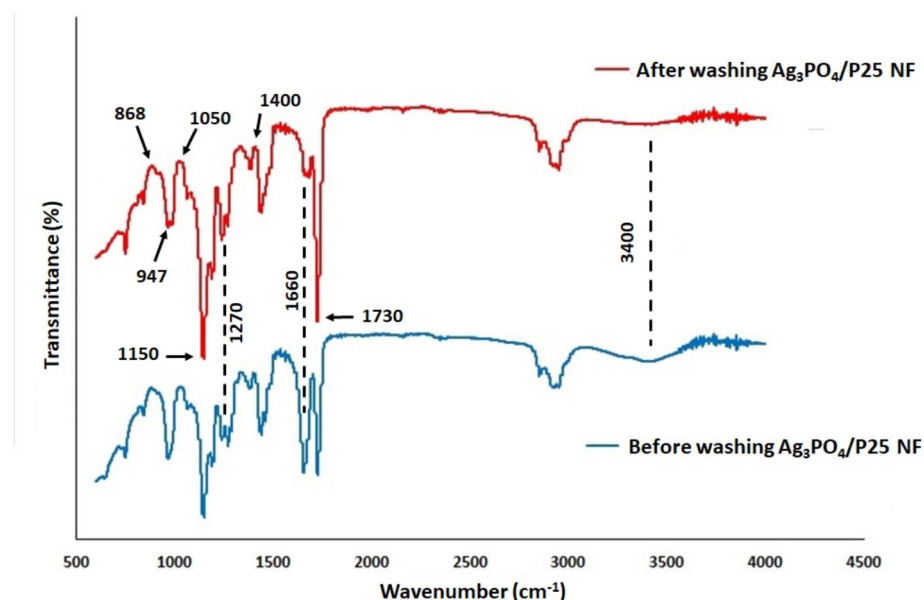


Figure 4. FTIR spectra of nanofibers before and after washing to remove PVP.

2.2. Band Gap Analysis

The band gap energy of $\text{Ag}_3\text{PO}_4/\text{P}25$ nanocomposite was determined by UV-visible absorption spectra in range of 200–1100 nm, as shown in Figure 5. From this scan, bandgap value can be evaluated by Tauc analysis using following equation:

$$\alpha h\nu = A(h\nu - E_g)^n \quad (1)$$

whereas: α = absorption coefficient, h = Planck constant, ν = light frequency, E_g = band gap energy, A = proportionality constant.

From this equation, the corresponding band gap value was calculated by extrapolating $(\alpha h\nu)^2$ vs. $(h\nu)$, where linear portion of $(\alpha h\nu)^2$ intercepts $h\nu$ axis at $\alpha = 0$ [22]. The band gap value is 2.45 eV for $\text{Ag}_3\text{PO}_4/\text{P}25$ nanocomposite, as shown in inset graph of Figure 5, which is quite comparable with the literature [23]. However, the calculated band gap value for commercial TiO_2 nanoparticles (P25) is 2.97 eV due to the 21 nm average particle size, as reported in a previous study [24].

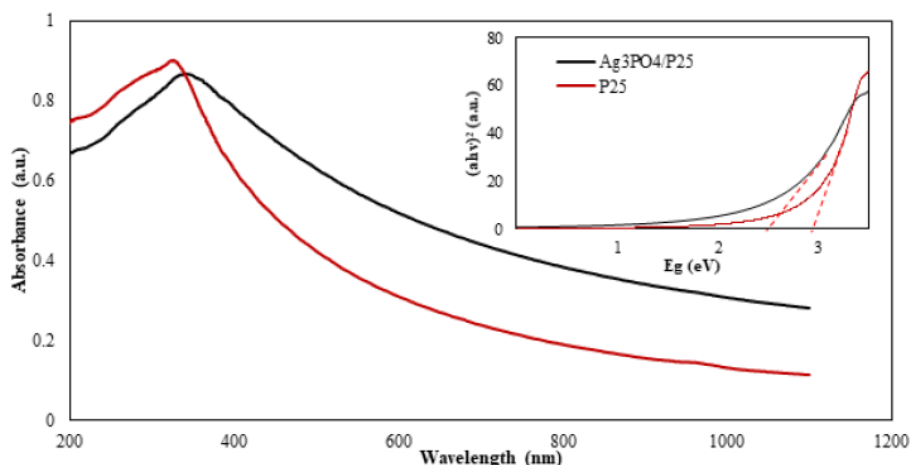


Figure 5. UV-visible spectra of P25 and $\text{Ag}_3\text{PO}_4/\text{P25}$ nanocomposite. Inset graph: Band gap determination using Tauc plot: data fitting to Equation (1).

2.3. Photocatalytic Degradation of Methyl Orange by $\text{Ag}_3\text{PO}_4/\text{P25}$ Nanofibers

Figure 6 depicts photodegradation of MO under simulated sunlight at room temperature. Prior to the irradiation experiment, NFs were pre-saturated in MO solution in the dark (-30 to 0 min) in order to get the adsorption capacity. All other conditions (pH, dye concentration, and temperature) remained same throughout the experiment. The experiment was repeated three times and average values were plotted. There was no significant change in dye color when treated with pure polymer NFs with a rate constant of $(0.9 \pm 0.01) \times 10^{-3} \text{ min}^{-1}$. This might be attributed to the lower adsorption of negatively charged MO on PMMA/PVP NFs, as stated in the literature [25]. But in the presence of $\text{Ag}_3\text{PO}_4/\text{P25}$ NFs, dye solution showed significant results, as the characteristic peak of MO at 465 nm declined significantly and nearly disappeared after 150 min of irradiation. The polymer NFs immobilized with 0.6% $\text{Ag}_3\text{PO}_4/\text{P25}$ nanoparticles exhibited 94% removal of MO as compared to 37% and 15% for only P25 and pure polymer blend NFs (PMMA/PVP), respectively. Meanwhile, 84% and 70% degradation of MO was achieved for polymer NFs anchored with 0.4% and 0.2% nanoparticles, respectively. This decrease in efficiency was due to fewer available active sites on the surface of polymer NFs. The rate constant value was also calculated using first-order kinetic equation. After 150 min of irradiation, rate constant values of $(5.9 \pm 0.03) \times 10^{-3}$, $(4.9 \pm 0.02) \times 10^{-3}$, and $(4.1 \pm 0.04) \times 10^{-3} \text{ min}^{-1}$ were achieved for PMMA to $\text{Ag}_3\text{PO}_4/\text{P25}$ ratios (1:0.6), (1:0.4) and (1:0.2), respectively. The photocatalytic efficiency of pure P25 NFs was also evaluated under same conditions and subsequently resulted in much lower degradation $(2.3 \pm 0.04) \times 10^{-3} \text{ min}^{-1}$ as compared to $\text{Ag}_3\text{PO}_4/\text{P25}$ NFs. The dye degradation mechanism has already explained by some researchers [21]. However, in this study, superior photocatalytic activity of $\text{Ag}_3\text{PO}_4/\text{P25}$ NFs (after PVP removal) could be attributed to surface exposed nanoparticles which took part in enhanced photodegradation [20], while the lower photocatalytic activity of P25 NFs was attributed to weak sunlight absorption of Degussa-P25. Besides this, the self-photosensitized activity of adsorbed dye on surface of P25 NFs might be the reason for photodegradation of MO under simulated sunlight [26].

2.4. Stability of $\text{Ag}_3\text{PO}_4/\text{P25}$ Nanofibers

An important parameter for a practically viable photocatalyst is its stability during a photocatalytic reaction. According to the literature, Ag_3PO_4 has some stability issues in practical application due to the presence of sacrificial reagents that might have resulted in its partial reduction in metallic silver [27]. Consequently, the photocatalytic and structural stability of Ag_3PO_4 is a major challenge for its practical application. To determine the consistency of prepared NFs, NFs were reused in five successive MO degradation experiments. These experiments were performed by used NFs with PMMA: Ag_3PO_4 (1:0.6) in fresh MO (10 mg/L) solution, as shown in Figure 7. All experimental parameters were same

for stability test. The obtained results show that there was no significant loss in photocatalytic ability of $\text{Ag}_3\text{PO}_4/\text{P}25$ NFs to degrade MO. At neutral pH, dye solution showed significant results with a rate constant value of $(5.9 \pm 0.03) \times 10^{-3} \text{ min}^{-1}$, which remained stable $(5.8 \pm 0.05) \times 10^{-3} \text{ min}^{-1}$ at the end of fifth run with ability to degrade organic pollutants for several cycles. These results are in accordance with the findings of Yu et al. [28], where they prepared stable Ag_3PO_4 -PAN composite nanofibers by electrospinning. These findings suggest PMMA as a robust hosting matrix for the polishing of dyeing effluent.

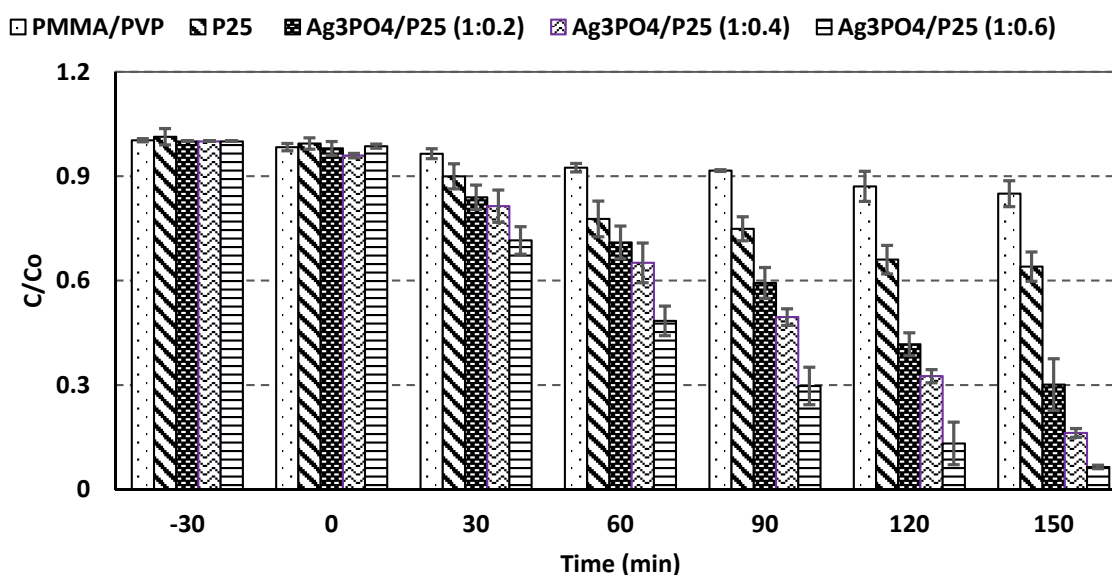


Figure 6. Methyl orange (MO) photocatalytic degradation under simulated sunlight using PMMA/PVP, P25, PMMA: $\text{Ag}_3\text{PO}_4/\text{P}25$ ratio (1:0.2) (1:0.4) and (1:0.6).

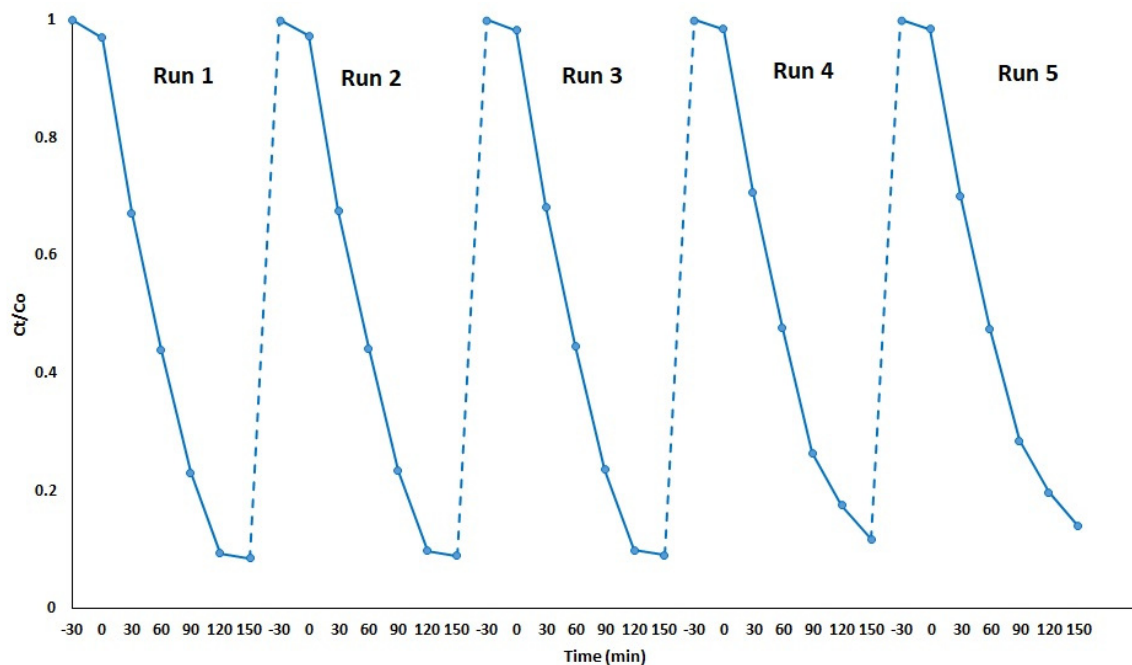


Figure 7. Recycling performance of electrospun nanofibers for photocatalytic degradation of methyl orange (MO) under simulated sunlight using PMMA: $\text{Ag}_3\text{PO}_4/\text{P}25$ (1:0.6).

2.5. Antibacterial Efficiency of $\text{Ag}_3\text{PO}_4/\text{P25}$ Composite Nanofibers

Antibacterial efficiency of as synthesized $\text{Ag}_3\text{PO}_4/\text{P25}$ NFs was assessed by quantification of *E. coli* after contacting with $\text{Ag}_3\text{PO}_4/\text{P25}$ and Degussa P25 NFs for 1 h in dark. $\text{Ag}_3\text{PO}_4/\text{P25}$ NFs showed excellent results for the inactivation of *E. coli* with an initial concentration of 10^6 CFU/mL , as compared to P25 NFs. The removal of bacteria in plates with no NFs (control) might be attributed to some natural or environmental factors. P25 NFs did not show any remarkable antibacterial activity in the dark; however, a more pronounced effect was revealed by $\text{Ag}_3\text{PO}_4/\text{P25}$ NFs, as one could not find any single bacterial cell there, as shown in Figure 8a,b. In the presence of light, antimicrobial activity would be the result of reactive oxygen species (ROS), as reported by Al-Ghafri et al. [29], where active OH° radicals from electron–hole pairs are capable to react with cellular proteins, cell membranes, and also DNA which ultimately cause death of bacterial cell. While in the dark, oxidation state of silver and the release of ionic silver in solution would be responsible for bacterial inactivation [30], as they attach themselves with the thiol group (SH), resulting in destabilization of cell wall and membranes, followed by disrupting adenosine triphosphate (ATP) synthesis and DNA replication [31]. In this study, surface-exposed $\text{Ag}_3\text{PO}_4/\text{P25}$ nanoparticles might have direct contact with the bacterial strain, resulting in higher antibacterial activity without the fear of losing nanoparticles in the solution.

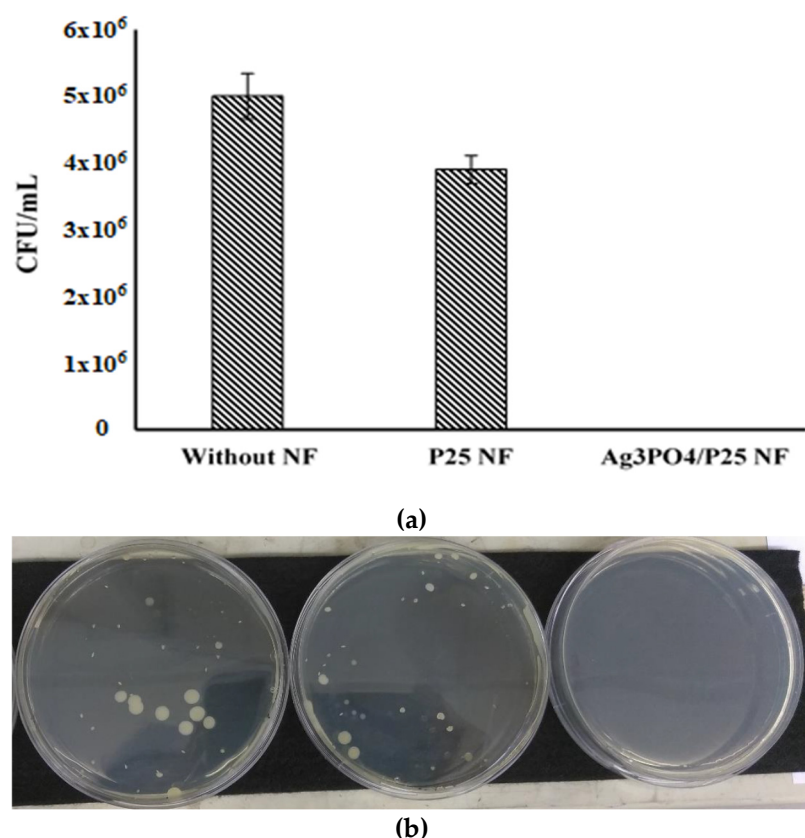


Figure 8. (a) and (b): The *E. coli* colonies without nanofibers and after contact with P25 and $\text{Ag}_3\text{PO}_4/\text{P25}$ nanofibers (inoculum level 10^6 CFU/mL).

2.6. Tertiary Treatment of Synthetic Textile Secondary Effluent Using Plug Flow Reactor (PFR)

Effluent from textile industry consists of an amalgam of dyes and inorganic salts. Due to this, treatment of real wastewater is difficult as compared to individual dye degradation at the lab scale. Biological as well as membrane processes are widely used treatment technologies in the textile industries. These processes are capable enough to meet the National Environmental Quality Standards (NEQS) of Pakistan Environmental Protection Agency (Pak-EPA). However, for reuse purposes, effluent discharge from the dyeing unit should be completely transparent in order to meet the target of zero

discharge of hazardous chemicals (ZDHC) [32]. Some of the dyes, depending on their ionic state and molecular weight, might be easily removed by the activated sludge process, but the complete mineralization of dye molecules is quite difficult without polishing with the photodegradation process. However, it was demonstrated [33] that the existence of inorganic salts significantly influences the photocatalytic process, resulting in deteriorating dye removal efficiency.

The efficiency of synthesized NFs was evaluated for the polishing of UASB-treated effluent [13]. Samples were analyzed in terms of turbidity removal, dye degradation and TOC removal as shown in Table 1 using Standard Methods [34].

Table 1. Parameters studied for polishing of synthetic secondary effluent.

Flow Rate (mL/h)	Turbidity (NTU)	Color Removal (%)	TOC (%)
5	4.80	MO: 21.0 MB: 66.0	86.00
7	5.18	MO: 19.0 MB: 53.9	82.69
9	6.17	MO: 16.7 MB: 53.4	54.63

The turbidity of influent (synthetic secondary effluent) was 9.76 ± 3.2 NTU, measured by turbidity meter, and better removal efficiency was obtained at a lower flow rate. The deterioration in removal efficiency was observed as flow rate was increased from 5 to 9 mL/h. An almost 50% reduction in turbidity was observed, while the decline in dye degradation (MB and MO) was detected due to the presence of inorganic salts in a complex nature synthetic effluent as well as the loss of available active sites [35]. From Table 1, at the lowest flow rate (5 mL/h), only 66% removal of MB was observed as compared to MO (insignificant removal ~21%). In synthetic simulated textile wastewater, MO exhibited much lower removal as compared to individual dye solution (Section 2.3). The lower removal efficiency of both dyes in a mixed solution is attributed to the complex mixture of MB and MO, while the insignificant removal of MO might be the outcome of basic pH ~7.8 (not feasible for MO degradation) in addition to complex mixture [36]. Total organic carbon (TOC) was analyzed using a TOC analyzer (TOC-V_{CSH}, Shimadzu, Japan), resulting in a maximum 86% removal in terms of mineralization at lower flowrate of 5 mL/h.

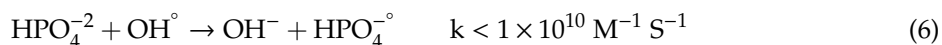
In the context of lower efficiency, despite the abovementioned reasons, accumulation of a salt layer (Cl^- ion) on the surface of photocatalyst affects the photocatalytic efficiency, making the approach of target pollutant (dye molecules) to photocatalyst more difficult. In fact, Cl^- ions might be easily adsorbed on the surface of polymer NFs and compete for active sites in the presence of organic pollutants. Similarly, these ions contest with oxygen for electrons and diminish the formation of superoxide radicals, ultimately resulting in lower photocatalytic degradation. The hole scavenging property of Cl^- ions also makes photodegradation more difficult in the presence of inorganic salts as follows [37]:



Besides this, Cl° radicals are also competent to oxidize organic pollutants in the same way as OH° radicals but at a lower rate due to less oxidizing power as compared to OH° [38].

Similarly, the effect of potassium dihydrogen phosphate on photocatalytic degradation is the consequence of predominant species (HPO_4^{2-}) in basic medium. These dominant hydrogen phosphates

(HPO_4^{2-}) resulted in a lower oxidation process by scavenging OH° radicals in order to form anionic radicals ($\text{HPO}_4^{\cdot-}$), as shown in equation below [39]:



In short, the ample amount of these inorganic salts in real wastewater with basic pH would seriously decrease the photocatalytic degradation of dye molecules for the following reasons:

- (1) Attenuating the light penetration due to deeper solution induced by inorganic salts and dyes mixture, taking part as an inner filter [40].
- (2) Scavenging the OH° radicals as well as other oxidizing species.
- (3) Competition among inorganic salts and dye molecules for adsorption on active sites of the photocatalyst [41].

3. Materials and Methods

3.1. Reagents

All reagents were used as received unless specified. Titania nanoparticles (P25, ≥99.5% purity), Sodium Phosphate (Na_3PO_4) (ACS reagent, 96% purity), poly(methyl methacrylate) (PMMA) (Mol. wt. 350,000 Da), poly(vinyl pyrrolidone) (PVP) (Mol. wt. 55,000 Da). N-N dimethyl acetamide (DMAC) (≥99.5% purity), methyl orange (MO) (85% purity), methylene blue (MB) (≥82% purity), glucose ($\text{C}_6\text{H}_{12}\text{O}_6$) (ACS reagent, ≥99.5% purity), ammonium chloride (NH_4Cl) ACS reagent, ≥99.5% purity, potassium dihydrogen phosphate (KH_2PO_4) (99% purity) and sodium bicarbonate (NaHCO_3) (ACS reagent, 99.7% purity) were purchased from Sigma Aldrich (St. Louis, MO, USA). All solutions were prepared in deionized water produced by a Millipore (Milli-Q® Academic) water purification system.

3.2. Preparation of $\text{Ag}_3\text{PO}_4/\text{P25}$ Composite

$\text{Ag}_3\text{PO}_4/\text{P25}$ composite was prepared by the previously reported in situ precipitation method [5]. Briefly, 1.59 g of commercial Degussa (P25) was dispersed in 50 mL distilled water and ultrasonicated for 10 min. After sonication, 3.057 g of AgNO_3 was immediately added to the above suspension and magnetically stirred until a homogeneous suspension was obtained. Afterwards, previously dissolved 0.98 g Na_3PO_4 in 50 mL distilled water was added dropwise and stirred for 5 h at room temperature. The color of the mixture changed from white to yellow immediately after adding the Na_3PO_4 solution. Then, the composite was filtered, washed with distilled water several times, and dried in a vacuum oven at 60 °C overnight. The resulting material was kept in airtight jars for further use.

3.3. Preparation of $\text{Ag}_3\text{PO}_4/\text{P25}$ Nanofibers

To prepare $\text{Ag}_3\text{PO}_4/\text{P25}$ electrospun nanofibers, PMMA (12 wt %) and PVP (6 wt %) were first dissolved in 10 mL DMAC solvent (PMMA to PVP ratio remained constant in this study). Then, the desired amount of $\text{Ag}_3\text{PO}_4/\text{P25}$ powder was added into the polymer solution and stirred overnight. The homogenized solution was filled in 10 mL plastic syringe with a diameter of 14.53 mm. A voltage of 13 kV was applied to the positive electrode, i.e., stainless-steel needle on a syringe, while the receiving surface, a stainless-steel plate collector lined with aluminum foil, was grounded. The receiving surface was placed 15 cm away from the needle tip. The electrospun solution was supplied using a syringe pump (NE-300, Scientific Instrument Services, Inc, Ringoes, NJ, USA) at a flowrate of 0.5 mL/h and the electrospinning process was operated for 11 h at room temperature. Immediately after the electrospinning process, the fibrous mat was peeled off from the receiving surface and dipped in deionized water overnight for almost 12 to 18 h at 25 °C in order to dissolve PVP and dried in a vacuum oven at 65 °C to get NFs having nanoparticles exposed surface. The same procedure was used for electrospun solutions with PMMA to $\text{Ag}_3\text{PO}_4/\text{P25}$ ratios of 1:0.2, 1:0.4, and 1:0.6 and denoted as $\text{Ag}_3\text{PO}_4/\text{P25}$ (1:0.2), $\text{Ag}_3\text{PO}_4/\text{P25}$ (1:0.4), and $\text{Ag}_3\text{PO}_4/\text{P25}$ (1:0.6), respectively. For the control

experiments, bi-polymer (PMMA and PVP) NFs without photocatalyst were also prepared by the same procedure. Pure P25 NFs (P25 was taken in same ratio as that used in preparation of the $\text{Ag}_3\text{PO}_4/\text{P25}$ composite) were also prepared for comparison.

3.4. Material Characterization

In this study, NFs with PMMA to $\text{Ag}_3\text{PO}_4/\text{P25}$ ratio (1:0.6) were used for structural as well as morphological analysis. The surface morphology of prepared NFs was determined using scanning electron microscopy (SEM) (FEI Quanta 400F, Hillsboro, OR., USA) equipped with the Nordlys 2 Electron Backscatter Diffraction (EBSD) camera. The samples were coated with gold using the sputtering technique so as to avoid the electron beam charging of polymers and placed on an aluminum SEM stub for examination. Energy dispersive X-ray spectroscopy (EDXS) was used to determine the elemental composition of samples. Fourier transform infrared spectroscopy (FTIR) analysis was also performed in the range of 450 to 4000 cm^{-1} to characterize surface functional groups on NFs. Before the electrospinning process, UV-visible absorption spectra of $\text{Ag}_3\text{PO}_4/\text{P25}$ were also analyzed in order to clarify the optical properties of synthesized nanocomposite.

3.5. Photocatalytic Degradation Study

The photocatalytic activity of P25 electrospun NFs (in the form of mat) was evaluated using MO, a commonly studied azo dye, as a model dye contaminant. About 65–70% of the dyes used in the textile industry are azo dyes [42]. Batch photocatalytic degradation experiments were carried out in a Luzchem Photoreactor (LZC-4V Research, Inc., Ottawa, ON Canada) equipped with six 8W fluorescent (F8T5/D-T5, Eiko, Shawnee, KS, USA) lamps (source of simulated daylight), mounted on the top of the reaction chamber and having a wavelength in the range of 450–650 nm, comparable to natural sunlight. While the total intensity used in experiment was 3.1 mW/cm^2 , measured by a lightmeter-850009 (Control Company, Friendswood, TX, USA) with a traceable photosensor. Three glass beakers (replicate samples), each containing 25 mL MO solution (10 mg/L concentration), were placed in the photoreactor, 13 cm below the lamps. As-synthesized NFs were cut into rectangular coupons $2 \times 2 \text{ cm}^2$ in size ($\sim 0.05 \text{ g}$ in weight) and hung in the beaker using steel wire. Prior to irradiation, dye solutions were magnetically stirred in dark for 30 min in order to establish the adsorption–desorption equilibrium. Once irradiation started, samples were collected from each beaker at predetermined time intervals to analyze the remaining MO concentration by measuring absorbance at 465 nm using a dual beam UV-Vis spectrophotometer (UV-2550, Shimadzu, Tokyo, Japan). Decoloration using bi-polymer (PMMA and PVP) NFs without $\text{Ag}_3\text{PO}_4/\text{P25}$ nanoparticles was also evaluated under the same conditions as the control experiments. The stability of these NFs was assessed over five successive MO degradation experiments. MO degradation fits the first order kinetic model and the equation is expressed as [43]:

$$\ln \frac{C}{C_0} = -kt \quad (7)$$

where C_0 and C are the initial and final concentrations after time t , respectively, and k is the rate constant.

3.6. Evaluation of Antibacterial Activity

The antibacterial efficacy of electrospun NFs immobilized with 0.6 wt% nanoparticles was evaluated using a common Gram-negative bacterium *Escherichia coli* K12 as model microorganism. The bacterial culture was grown in LB broth at 37 °C for 16 h and washed three times using phosphate-buffer saline (PBS) by centrifugation. The cells were then re-suspended in 0.1 M PBS to obtain a concentration of 10^6 CFU/mL .

Electrospun NFs of the same size, as mentioned above, were placed in a six-well cell culture plates with 10^6 CFU/mL *E. coli* suspension to each sample well. The plates were then incubated for 1 h in the dark at 37 °C on a shaker at 90 rpm. After incubation, the bacterial suspension in each

well was sampled to determine the number of viable *E. coli* by the spread plate count (SPC) method. Each activity was repeated three times.

3.7. Plug Flow Reactor (PFR) Design and Operational Conditions

A small bench scale plug flow reactor (effective volume of 3.4 mL) was designed and tested at various flow rates for the polishing of secondary synthetic effluent (treated from UASB). Also, the effect of inorganic salts was investigated upon photocatalytic degradation. The PFR comprised of 19 channels which were engraved in an acrylic sheet. The $\text{Ag}_3\text{PO}_4/\text{P25}$ NF mat (1:0.6 polymer to nanoparticles ratio) as a photocatalyst was sealed between the silicon substrate and an acrylic sheet. Synthetic wastewater consisting of inorganic salts along with the MB and MO mixture was pumped into the PFR through a syringe pump (NE-300, Scientific Instrument Services, Inc, Ringoes, NJ, USA). The PFR set up was placed in a photocatalytic reactor (specification in Section 3.5) for irradiation. For inorganic contents, the measured amounts of Cl^- and PO_4^{3-} precursors were used in the preparation of synthetic feed along with the MB and MO mixture. The pH was adjusted to 7.8 (close to the pH of textile wastewater). The composition of synthetic feed is given in Table 2. Wastewater was allowed to pass through channels at various flow rates (5, 7 and 9 mL/h) and irradiated by lamps mounted in the photocatalytic reactor. The experiment was continued for each flow rate until sufficient treated effluent was achieved coming from PFR. The pictorial view of the photoreactor chamber along with the lab-scale PFR is presented in Figure 9.

Table 2. Composition of pretreated simulated textile effluent.

Chemicals	Formula	Concentration (mg/L)
Dextrose (glucose)	$\text{C}_6\text{H}_{12}\text{O}_6$	150
Ammonium chloride	NH_4Cl	380
Potassium dihydrogen phosphate	KH_2PO_4	43
Methyl orange (MO)	$\text{C}_{14}\text{H}_{14}\text{N}_3\text{NaO}_3\text{S}$	10
Methylene blue (MB)	$\text{C}_{16}\text{H}_{18}\text{ClN}_3\text{S}$	10

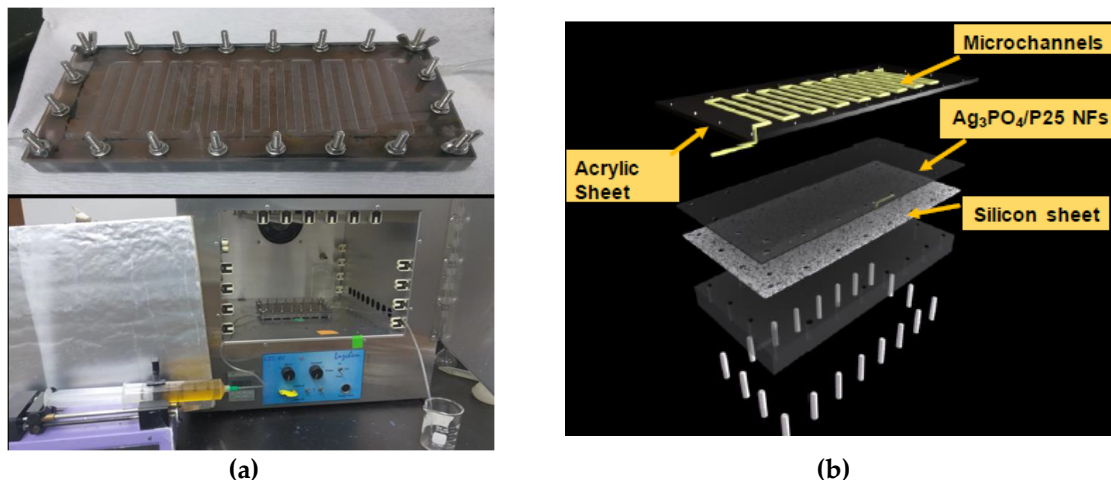


Figure 9. Pictorial view of Luzchem photoreactor (a) and lab-scale plug flow reactor (b).

4. Conclusions

Electrospun nanofibers using a polymer blend (PMMA-PVP) with an embedded $\text{Ag}_3\text{PO}_4/\text{P25}$ composite were prepared by electrospinning, followed by the removal of one polymer via selective dissolution. The embedded active $\text{Ag}_3\text{PO}_4/\text{P25}$ composite in PMMA exhibited an advantage of strong immobilizing power with no need to recover the nanoparticles after treatment. These NFs exhibited excellent performance for the degradation of MO (in the case of individual dye degradation

experiments) with a stable rate constant where efficiency was not lower than 85% at the end of fifth run. Also, these polymeric NFs revealed an important role in the destruction of microorganisms (*E. coli*), signifying their potential in water purification.

The polishing of secondary treated effluent was also achieved successfully, keeping in view the effect of inorganic salts on photocatalytic degradation. A lower flow rate (5 mL/h) resulted in maximum TOC and turbidity removal rates of 86% and 50%, respectively. However, the decline in dye degradation (MB and MO) was ascribed to the presence of inorganic salts in a complex synthetic effluent, specifically due to the loss of active sites and scavenging of OH[•] radicals. In short, these NFs were found to be a stable material that could yield a new horizon in designing electrospun NFs towards energy as well as environmental applications.

Author Contributions: Conceptualization by Z.H., S.J.K. and Q.L.; methodology by Z.H.; validation by S.J.K. and Q.L.; formal analysis by Z.H., C.-G.L., X.H. and H.J.; investigation by Z.H.; data curation by Z.H.; writing—original draft preparation by Z.H.; writing—review and editing by S.J.K., Q.L., Y.J. and N.M.A.; visualization by Z.H.; supervision by S.J.K. All authors have read and agreed to the published version of the manuscript.

Funding: This research was funded by Higher Education Commission (HEC), Pakistan for providing financial support (No: 1-8/HEC/HRD/2016/6383).

Acknowledgments: Authors wish to thank RICE University Houston, TX 77005, USA for providing lab facilities and National University of Sciences and Technology (NUST), H-12 Sector, Islamabad, Pakistan to carry out this research work successfully.

Conflicts of Interest: The authors declare no conflict of interest.

References

- Zhang, Z.-G.; Liu, H.; Wang, X.-X.; Zhang, J.; Yu, M.; Ramakrishna, S.; Long, Y.-Z.; Zhang, Z.-G.; Liu, H.; Wang, X.-X.; et al. One-Step Low Temperature Hydrothermal Synthesis of Flexible TiO₂/PVDF@MoS₂ Core-Shell Heterostructured Fibers for Visible-Light-Driven Photocatalysis and Self-Cleaning. *Nanomaterials* **2019**, *9*, 431. [[CrossRef](#)] [[PubMed](#)]
- Ali, I.; Kim, J.-O. Continuous-Flow Photocatalytic Degradation of Organics Using Modified TiO₂ Nanocomposites. *Catalysts* **2018**, *8*, 43. [[CrossRef](#)]
- Katal, R.; Kholghi Eshkalak, S.; Masudy-panah, S.; Kosari, M.; Saeedkhani, M.; Zarinejad, M.; Ramakrishna, S. Evaluation of Solar-Driven Photocatalytic Activity of Thermal Treated TiO₂ under Various Atmospheres. *Nanomaterials* **2019**, *9*, 163. [[CrossRef](#)] [[PubMed](#)]
- Giovannetti, R.; Rommozzi, E.; Zannotti, M.; D'Amato, C.A. Recent advances in graphene based TiO₂ nanocomposites (GTiO₂Ns) for photocatalytic degradation of synthetic dyes. *Catalysts* **2017**, *7*, 305. [[CrossRef](#)]
- Taheri, M.E.; Petala, A.; Frontistis, Z.; Mantzavinos, D.; Kondarides, D.I. Fast photocatalytic degradation of bisphenol A by Ag₃PO₄/TiO₂ composites under solar radiation. *Catal. Today* **2017**, *280*, 99–107. [[CrossRef](#)]
- Yi, Z.; Ye, J.; Kikugawa, N.; Kako, T.; Ouyang, S.; Stuart-williams, H.; Yang, H.; Cao, J.; Luo, W.; Li, Z.; et al. An orthophosphate semiconductor with photooxidation properties under visible-light irradiation. *Nat. Mater.* **2010**, *9*, 559–564. [[CrossRef](#)] [[PubMed](#)]
- Rosman, N.; Wan Salleh, W.N.; Aziz, F.; Ismail, A.F.; Harun, Z.; Bahri, S.S.; Nagai, K. Electrospun Nanofibers Embedding ZnO/Ag₂CO₃/Ag₂O Heterojunction Photocatalyst with Enhanced Photocatalytic Activity. *Catalysts* **2019**, *9*, 565. [[CrossRef](#)]
- Lee, C.G.; Javed, H.; Zhang, D.; Kim, J.H.; Westerhoff, P.; Li, Q.; Alvarez, P.J.J. Porous Electrospun Fibers Embedding TiO₂ for Adsorption and Photocatalytic Degradation of Water Pollutants. *Environ. Sci. Technol.* **2018**, *52*, 4285–4293. [[CrossRef](#)] [[PubMed](#)]
- Wang, C.; Yin, J.; Han, S.; Jiao, T.; Bai, Z.; Zhou, J.; Zhang, L.; Peng, Q. Preparation of Palladium Nanoparticles Decorated Polyethyleneimine/Polycaprolactone Composite Fibers Constructed by Electrospinning with Highly Efficient and Recyclable Catalytic Performances. *Catalysts* **2019**, *9*, 559. [[CrossRef](#)]
- Kalantari, M.; Du, R.; Ayrancı, C.; Boluk, Y. Effects of interfacial interactions and interpenetrating brushes on the electrospinning of cellulose nanocrystals-polystyrene fibers. *J. Colloid Interface Sci.* **2018**, *528*, 419–430. [[CrossRef](#)] [[PubMed](#)]

11. Doh, S.J.; Kim, C.; Lee, S.G.; Lee, S.J.; Kim, H. Development of photocatalytic TiO_2 nanofibers by electrospinning and its application to degradation of dye pollutants. *J. Hazard. Mater.* **2008**, *154*, 118–127. [[CrossRef](#)] [[PubMed](#)]
12. Cantarella, M.; Sanz, R.; Buccheri, M.A.; Ruffino, F.; Rappazzo, G.; Scalese, S.; Impellizzeri, G.; Romano, L.; Privitera, V. Immobilization of nanomaterials in PMMA composites for photocatalytic removal of dyes, phenols and bacteria from water. *J. Photochem. Photobiol. A Chem.* **2016**, *321*, 1–11. [[CrossRef](#)]
13. Haider, A.; Khan, S.J.; Saqib Nawaz, M.; Saleem, M.U. Effect of intermittent operation of lab-scale upflow anaerobic sludge blanket (UASB) reactor on textile wastewater treatment. *Desalin. Water Treat.* **2018**, *136*, 120–130.
14. Bairamis, F.; Konstantinou, I.; Petrakis, D.; Vaimakis, T. Enhanced Performance of Electrospun Nanofibrous $\text{TiO}_2/\text{g-C}_3\text{N}_4$ Photocatalyst in Photocatalytic Degradation of Methylene Blue. *Catalysts* **2019**, *9*, 880. [[CrossRef](#)]
15. Hu, D.; Xiao, Y.; Liu, H.; Wang, H.; Li, J.; Zhou, B. Loading of Au/Ag bimetallic nanoparticles within electrospun PVA/PEI nano fibers for catalytic applications. *Colloids Surf. A* **2018**, *552*, 9–15. [[CrossRef](#)]
16. Khan, M.Q.; Id, D.K.; Ullah, S.; Waqas, M.; Malik, A.; Abbasi, R.; Saito, Y.; Id, C.Z.; Kim, I.S. Self-Cleaning Properties of Electrospun PVA/ TiO_2 and PVA/ZnO Nanofibers Composites. *Nanomaterials* **2018**, *8*, 644. [[CrossRef](#)] [[PubMed](#)]
17. Keskinates, M.; Yilmaz, B.; Ulusu, Y.; Bayrakci, M. Electrospinning of novel calixarene-functionalized PAN and PMMA nanofibers: Comparison of fluorescent protein adsorption performance. *Mater. Chem. Phys.* **2018**, *205*, 522–529. [[CrossRef](#)]
18. Sundaran, S.P.; Reshma, C.R.; Sujith, A. Tailored design of polyurethane based fouling-tolerant nanofibrous membrane for water treatment. *New J. Chem.* **2018**, *42*, 1958–1972. [[CrossRef](#)]
19. Chaudhuri, B.; Mondal, B.; Ray, S.K.; Sarkar, S.C. A novel biocompatible conducting polyvinyl alcohol (PVA)-polyvinylpyrrolidone (PVP)-hydroxyapatite (HAP) composite scaffolds for probable biological application. *Colloids Surf. B Biointerfaces* **2016**, *143*, 71–80. [[CrossRef](#)] [[PubMed](#)]
20. Panthi, G.; Park, S.J.; Chae, S.H.; Kim, T.W.; Chung, H.J.; Hong, S.T.; Park, M.; Kim, H.Y. Immobilization of Ag_3PO_4 nanoparticles on electrospun PAN nanofibers via surface oximation: Bifunctional composite membrane with enhanced photocatalytic and antimicrobial activities. *J. Ind. Eng. Chem.* **2017**, *45*, 277–286. [[CrossRef](#)]
21. Saud, P.S.; Pant, B.; Twari, A.P.; Ghouri, Z.K.; Park, M.; Kim, H.Y. Effective photocatalytic efficacy of hydrothermally synthesized silver phosphate decorated titanium dioxide nanocomposite fibers. *J. Colloid Interface Sci.* **2016**, *465*, 225–232. [[CrossRef](#)] [[PubMed](#)]
22. Pattnaik, S.P.; Behera, A.; Martha, S.; Acharya, R.; Parida, K. Synthesis, photoelectrochemical properties and solar light-induced photocatalytic activity of bismuth ferrite nanoparticles. *J. Nanoparticle Res.* **2018**, *20*, 10. [[CrossRef](#)]
23. Liu, H.; Li, D.; Yang, X.; Li, H. Fabrication and characterization of $\text{Ag}_3\text{PO}_4/\text{TiO}_2$ heterostructure with improved visible-light photocatalytic activity for the degradation of methyl orange and sterilization of *E. coli*. *Mater. Technol.* **2019**, *34*, 192–203. [[CrossRef](#)]
24. Scarsella, M.; Bracciale, M.P.; de Caprariis, B.; de Filippis, P.; Petrullo, A.; Pronti, L.; Santarelli, M.L. Improved photocatalytic properties of doped titanium-based nanometric oxides. *Chem. Eng. Trans.* **2017**, *60*, 133–138.
25. Li, Y.; Zhao, H.; Yang, M. TiO_2 nanoparticles supported on PMMA nanofibers for photocatalytic degradation of methyl orange. *J. Colloid Interface Sci.* **2017**, *508*, 500–507. [[CrossRef](#)] [[PubMed](#)]
26. Yao, W.; Zhang, B.; Huang, C.; Ma, C.; Song, X.; Xu, Q. Synthesis and characterization of high efficiency and stable $\text{Ag}_3\text{PO}_4/\text{TiO}_2$ visible light photocatalyst for the degradation of methylene blue and rhodamine B. solutions. *J. Mater. Chem.* **2012**, *22*, 4050. [[CrossRef](#)]
27. Zhao, F.M.; Pan, L.; Wang, S.; Deng, Q.; Zou, J.J.; Wang, L.; Zhang, X. $\text{Ag}_3\text{PO}_4/\text{TiO}_2$ composite for efficient photodegradation of organic pollutants under visible light. *Appl. Surf. Sci.* **2014**, *317*, 833–838. [[CrossRef](#)]
28. Yu, H.; Jiao, Z.; Hu, H.; Lu, G.; Ye, J.; Bi, Y. Fabrication of Ag_3PO_4 -PAN composite nanofibers for photocatalytic applications 3. *R. Soc. Chem. Rev.* **2013**, *15*, 4802–4805. [[CrossRef](#)]
29. Al-Ghafri, B.; Lau, W.-J.; Al-Abri, M.; Goh, P.-S.; Ismail, A.F. Titanium dioxide-modified polyetherimide nanofiber membrane for water treatment. *J. Water Process. Eng.* **2019**, *32*, 100970. [[CrossRef](#)]

30. Piccirillo, C.; Pinto, R.A.; Tobaldi, D.M.; Pullar, R.C.; Labrincha, J.A.; Pintado, M.M.E.; Castro, P.M.L. Light induced antibacterial activity and photocatalytic properties of Ag/Ag₃PO₄-based material of marine origin. *J. Photochem. Photobiol. A Chem.* **2014**, *296*, 40–47. [[CrossRef](#)]
31. Dong, C.; Wang, Z.; Wu, J.; Wang, Y.; Wang, J.; Wang, S. A green strategy to immobilize silver nanoparticles onto reverse osmosis membrane for enhanced anti-biofouling property. *Desalination* **2017**, *401*, 32–41. [[CrossRef](#)]
32. Nimkar, U. Sustainable Chemistry: A Solution to the Textile Industry in a Developing World. *Curr. Opin. Green Sustain. Chem.* **2017**, *9*, 13–17. [[CrossRef](#)]
33. Wiszniewski, J.; Robert, D.; Surmacz-Gorska, J.; Miksch, K.; Malato, S.; Weber, J.-V. Solar photocatalytic degradation of humic acids as a model of organic compounds of landfill leachate in pilot-plant experiments: Influence of inorganic salts. *Appl. Catal. B Environ.* **2004**, *53*, 127–137. [[CrossRef](#)]
34. American Public Health Association. *APHA Method 4500-F: Standart Methods for the Examination of Water and Wastewater*; American Public Health Association: Washington, DC, USA, 2012.
35. Wang, H.; Huang, X.; Li, W.; Gao, J.; Xue, H.; Li, R.K.Y. TiO₂ nanoparticle decorated carbon nano fibers for removal of organic dyes. *Colloids Surf. A* **2018**, *549*, 205–211. [[CrossRef](#)]
36. Diantoro, M.; Kusumaatmaja, A.; Triyana, K. Study on Photocatalytic Properties of TiO₂ Nanoparticle in various pH condition. *J. Phys. Conf. Ser.* **2018**, *1011*, 012069.
37. Bouanimba, N.; Laid, N.; Zouaghi, R.; Sehili, T. Effect of pH and inorganic salts on the photocatalytic decolorization of methyl orange in the presence of TiO₂ P25 and PC500. *Desalin. Water Treat.* **2013**, 1–13. [[CrossRef](#)]
38. Kiwi, J.; Lopez, A.; Nadtochenko, V. Mechanism and Kinetics of the OH-Radical Intervention during Fenton Oxidation in the Presence of a Significant Amount of Radical Scavenger (Cl⁻). *Environ. Sci. Technol.* **2000**, *34*, 2162–2168. [[CrossRef](#)]
39. Zhu, X.; Nanny, M.A.; Butler, E.C. Effect of inorganic anions on the titanium dioxide-based photocatalytic oxidation of aqueous ammonia and nitrite. *J. Photochem. Photobiol. A Chem.* **2007**, *185*, 289–294. [[CrossRef](#)]
40. Grace, A.S.; Michael, S. Phytoplankton productivity in newly dug fish ponds within Lake Victoria wetlands (Uganda). *Afr. J. Environ. Sci. Technol.* **2010**, *4*, 365–370. [[CrossRef](#)]
41. Guillard, C.; Puzenat, E.; Lachheb, H.; Houas, A.; Herrmann, J.-M. Why inorganic salts decrease the TiO₂ photocatalytic efficiency. *Int. J. Photoenergy* **2005**, *7*, 1–9. [[CrossRef](#)]
42. Tayel, A.; Ramadan, A.R.; El Seoud, O.A. Titanium dioxide/graphene and titanium dioxide/graphene oxide nanocomposites: Synthesis, characterization and photocatalytic applications for water decontamination. *Catalysts* **2018**, *8*, 491. [[CrossRef](#)]
43. Aljeboree, A.M.; Alshirifi, A.N.; Alkaim, A.F. Kinetics and equilibrium study for the adsorption of textile dyes on coconut shell activated carbon. *Arab. J. Chem.* **2017**, *10*, S3381–S3393. [[CrossRef](#)]



© 2020 by the authors. Licensee MDPI, Basel, Switzerland. This article is an open access article distributed under the terms and conditions of the Creative Commons Attribution (CC BY) license (<http://creativecommons.org/licenses/by/4.0/>).